PCCP

RSC Publishing

PAPER

View Article Online
View Journal | View Issue

Cite this: *Phys. Chem. Chem. Phys.*, 2013, **15**, 10118

An *ab initio* variationally computed room-temperature line list for $^{32}S^{16}O_3$†

Daniel S. Underwood, Jonathan Tennyson and Sergei N. Yurchenko*

Received 22nd January 2013,
Accepted 19th March 2013

DOI: 10.1039/c3cp50303h

www.rsc.org/pccp

Ab initio potential energy and dipole moment surfaces are computed for sulfur trioxide (SO_3) at the CCSD(T)-F12b level of theory with appropriate triple-zeta basis sets. The analytical representations of these surfaces are used, with a slight correction, to compute pure rotational and rotation–vibration spectra of $^{32}S^{16}O_3$ using the variational nuclear motion program TROVE. The calculations considered transitions in the region 0–4000 cm^{-1} with rotational states up to $J = 85$. The resulting line list of 174 674 257 transitions is appropriate for modelling room temperature $^{32}S^{16}O_3$ spectra. Good agreement is found with the observed infrared absorption spectra and the calculations are used to place the measured relative intensities on an absolute scale. A list of 10 878 experimental transitions is provided in a form suitable for inclusion in standard atmospheric and planetary spectroscopic databases.

I Introduction

Sulfur trioxide (SO_3) is a stable, planar, symmetric molecule whose electronic ground state is a closed shell. On earth it is a pollutant produced from smoke-stacks and other industrial exhausts.[1] In the atmosphere SO_3 forms sulfuric acid with its association with acid rain. It is also corrosive inside combustion systems. In both cases the reactivity of SO_3 makes its production hard to monitor.[2] SO_3 is produced naturally on earth as part of volcanic emissions.[3] It is also thought to be a significant constituent of the atmosphere of Venus.[4]

The infrared vibration–rotation spectrum of $^{32}S^{16}O_3$ (henceforth referred to as SO_3) has been extensively investigated in a series of papers by Maki and co-workers.[5–11] Its "forbidden" rotational spectrum, for which centrifugal distortions can induce transitions, has been investigated using microwave Fourier-transform spectroscopy.[12] However, although these works provide an extensive list of measured line frequencies, none of them report absolute transition intensities.

There has been limited theoretical work on SO_3. Dorney *et al.*[13] reported force constants, while Martin[14] computed an *ab initio* quartic force field using coupled cluster methods and reported theoretical estimates for the band origins of the low-lying vibrational states. Again, neither of these works considered transition intensities.

The lack of any absolute transition intensities for SO_3 places severe limitations on the use of its infrared spectrum for remote sensing applications or inclusion of this data in standard atmospheric and planetary spectroscopic databases.[15,16] In this work we report the calculation of a new *ab initio* PES and associated dipole moment surface (DMS) for SO_3. These are used to not only produce theoretical spectra for $^{32}S^{16}O_3$, but also to place the relative intensity measurements of its infrared spectrum on an absolute scale.

II The potential energy and dipole moment surfaces

The *ab initio* PES was computed using the recently-proposed explicitly correlated F12 singles and doubles coupled cluster method including a perturbational estimate of connected triple excitations, CCSD(T)-F12b,[17] in conjunction with the corresponding F12-optimized correlation consistent basis sets, namely the valence correlation-consistent functions aug-cc-pVTZ-F12 and aug-cc-pV(T+d)Z-F12 for oxygen and sulfur, respectively.[18] We also utilized the OptRI,[19] cc-pV5Z/JKFIT[20] and aug-cc-pwCV5Z/MP2FIT[21] auxiliary basis sets for evaluating the many-electron integrals, the exchange and Fock operators, and the remaining electron repulsion integrals, respectively. The value of the geminal Slater exponent β was chosen as 1.2. Relativistic corrections were introduced as scalar relativistic effects and the diagonal Born–Oppenheimer corrections (DBOCs) were also computed. Molpro.2010[22] was employed for all electronic structure calculations. We used a grid of 13 000 points with the bond lengths r_i ($i = 1,2,3$) ranging from 1.1 to 2.0 Å, the interbond angles α_k ($k = 1,2,3$)

Department of Physics and Astronomy, University College London, Gower Street, London WC1E 6BT, UK. E-mail: s.yurchenko@ucl.ac.uk

† Electronic supplementary information (ESI) available. See DOI: 10.1039/c3cp50303h

Table 1 Convergence of the basis set viewed for some vibrational band centres (cm^{-1}) for $^{32}S^{16}O_3$

	Obs.[8]	P_{max} = 10	P_{max} = 12	P_{max} = 14
ν_1	1064.92	1065.83	1065.75	1065.74
ν_2	497.57	498.48	498.48	498.48
ν_3	1391.52	1387.63	1387.45	1387.43
ν_4	530.09	528.61	528.59	528.58
$2\nu_3(l_3 = 0)$	2766.40	2759.61	2759.12	2758.75
$2\nu_3(l_3 = 2)$	2777.87	2770.70	2770.29	2769.95
$2\nu_2$	995.02	995.43	995.35	995.35
$2\nu_4(l_4 = 0)$	1059.81	1057.10	1056.50	1056.44
$2\nu_4(l_4 = 2)$	1060.45	1057.86	1057.38	1057.33
$\nu_2 + \nu_4(l_4 = 1)$	1027.90	1027.58	1027.35	1027.33
$\nu_1 + \nu_4(l_4 = 1)$	1593.69	1593.82	1593.36	1593.30
$3\nu_4(l_4 = 1)$	1589.81	1587.64	1586.46	1586.30
$3\nu_4(l_4 = 3)$	1591.10	1587.61	1586.43	1586.27
$\nu_1 + \nu_2$	1560.60	1565.51	1565.33	1565.32
$\nu_2 + 2\nu_4(l_4 = 0)$	1557.88	1556.38	1555.59	1555.47
$\nu_2 + 2\nu_4(l_4 = 2)$	1558.52	1557.12	1556.45	1556.37
$2\nu_2 + \nu_4(l_4 = 1)$	1525.61	1524.81	1524.48	1524.46
$3\nu_2$	1492.35	1449.81	1490.76	1490.76
$\nu_2 + \nu_3(l_3 = 1)$	1884.57	1881.82	1881.53	1881.51
$3\nu_3(l_3 = 1)$	4136.39	4138.88	4126.78	4125.92

between 70 and 123°, and the inversion angle $\bar{\rho}$ between 0 and 50°. Grid points were specified based on an algorithm which produced a higher concentration of points close to the equilibrium position in a coupled-cluster manner. Each point was processed using an MP2 calculation as a further filter, and those producing an MP2 result of 50 000 cm^{-1} or higher were disregarded. This grid is sufficient to cover energies up to 40 000 cm^{-1} above the minimum. We note that CCSD(T) is not very reliable for the higher energy regions which approach dissociation. The T1 diagnostic test[23] was applied to all *ab initio* points to ensure that the CCSD(T) treatment is adequate for all geometries considered.

This PES is represented by an analytical form given by the expansion[24]

$$\begin{aligned} V(\xi_1,\xi_2,\xi_3,\xi_{4a},\xi_{4b};\sin\bar{\rho}) &= V_e + V_0(\sin\bar{\rho}) + \sum_j F_j(\sin\bar{\rho})\xi_j \\ &+ \sum_{j\le k} F_{jk}(\sin\bar{\rho})\xi_j\xi_k \\ &+ \sum_{j\le k\le l} F_{jkl}(\sin\bar{\rho})\xi_j\xi_k\xi_l \\ &+ \sum_{j\le k\le l\le m} F_{jklm}(\sin\bar{\rho})\xi_j\xi_k\xi_l\xi_m \end{aligned} \quad (1)$$

in the coordinates ξ_k:

$$\xi_k = 1 - \exp(-a(r_k - r_e)), \quad k = 1,2,3, \quad (2)$$

$$\xi_{4a} = \frac{1}{\sqrt{6}}(2\alpha_1 - \alpha_2 - \alpha_3), \quad (3)$$

$$\xi_{4b} = \frac{1}{\sqrt{2}}(\alpha_2 - \alpha_3), \quad (4)$$

$$\sin\bar{\rho} = \frac{2}{\sqrt{3}}\sin[(\alpha_1 + \alpha_2 + \alpha_3)/6], \quad (5)$$

where

$$V_0(\sin\bar{\rho}) = \sum_{s=1} f_0^{(s)}\,(\sin\rho_e - \sin\bar{\rho})^s \quad (6)$$

and

$$F_{jk\ldots}(\sin\bar{\rho}) = \sum_{s=0} f_{jk\ldots}{}^{(s)}\,(\sin\rho_e - \sin\bar{\rho})^s. \quad (7)$$

Here $\sin\rho_e$ is the equilibrium value of $\sin\bar{\rho}$, a is a molecular parameter, and the quantities $f_0^{(s)}$ and $f_{jk\ldots}{}^{(s)}$ in eqn (6) and (7) are expansion coefficients. The linear stretching terms $f_1^{(0)} = f_2^{(0)} = f_3^{(0)}$ are fixed to zero so that the minimum of $V(\xi_1,\xi_2,\xi_3,\xi_{4a},\xi_{4b};\sin\bar{\rho})$ is at r_e. The asymmetric bending linear terms $f_{4a}{}^{(0)}$ and $f_{4b}{}^{(0)}$ also vanish because of the symmetric arguments. The same form has been used to represent the PESs of NH_3, PH_3, SbH_3, NH_3^+, and BiH_3.[25–28] The potential parameters $f_{jk\ldots}{}^{(s)}$ were obtained through a weighted least squares fit to the *ab initio* points with a root-mean-square (rms) error of 0.067 cm^{-1}. Weight factors were set using the expression suggested by Partridge and Schwenke:[29]

$$w_i = N\frac{\tanh\left[-0.0005\text{ cm}\times\left(V_i - 16\,000\text{ cm}^{-1}\right)\right] + 1.00000002}{2.00000002}, \quad (8)$$

where N is a normalization factor defined by $\sum_i w_1 = 1$ and V_i is the *ab initio* energy at the ith geometry (in cm^{-1}), measured relative to the equilibrium energy. These weight factors favor the energies below 16 000 cm^{-1}. The *ab initio* equilibrium geometry r_e^{ai} as obtained from the fit is 1.42044 Å. This can be compared with an experimentally derived value 1.41732 Å.[6]

The quality of the *ab initio* PES can be assessed by calculating the fundamental term values of the molecule. Employing the variational approach TROVE[30] (see below) with the *ab initio* PES we obtain 1073.56, 499.89, 1396.75, and 529.74 cm^{-1} for ν_1, ν_2, ν_3, and ν_4, respectively. The corresponding experimentally derived values are listed in Table 1. While the bending modes are reproduced reasonably well, the stretching fundamental term values exhibit large deviations from the experiment, 5–9 cm^{-1}. In order to improve the quality of the stretching modes we have used the following morphing procedure.[31] We re-expand the *ab initio* PES (1) around an intermediate reference geometry r^{ref}, which is selected close to r_e^{ai}. This introduces a smooth deformation of all values $f_{jk\ldots}{}^{(s)}$ based on one adjusting parameter r^{ref} only. The linear stretching terms $f_1^{(0)}$, $f_2^{(0)}$, and $f_3^{(0)}$ that appear in this representation are dropped out again by setting them to zero. The reference geometry r^{ref}, which is now also an 'equilibrium' geometry is then replaced by the experimentally derived value 1.41732 Å. We found that the experimental rotational energies of $^{32}S^{16}O_3$ (ref. 8) are best reproduced by the latter value. With this 'morphed' PES the deviations of the theoretical fundamental term values become 1.0, 0.9, 4.0, and 1.5 cm^{-1} for ν_1, ν_2, ν_3, and ν_4, respectively. Table 2 illustrates the improvement in the rotational energies achieved, where a selection of experimentally derived pure rotational term values reported by Maki *et al.*[8] is compared to corresponding values obtained using the *ab initio* and morphed PESs. The latter PES

Table 2 Rotational term values (cm^{-1}) of $^{32}S^{16}O_3$ in the ground vibrational state: the theoretical term values were obtained using the *ab initio* (A) and morphed (M) PESs; the experimentally derived values (Obs.) are from ref. 8

J	K	Obs.	Calc. (A)	Calc. (M)
2	0	2.0912	2.0826	2.0916
3	3	2.6115	2.6007	2.6119
4	0	6.9707	6.9419	6.9718
4	3	5.3998	5.3775	5.4006
5	3	8.8852	8.8484	8.8864
6	3	13.0675	13.0134	13.0694
6	6	8.3548	8.3201	8.3559
7	3	17.9467	17.8724	17.9493
7	6	13.2342	13.1794	13.2360
8	0	25.0935	24.9897	25.0972
8	3	23.5228	23.4255	23.5263
8	6	18.8106	18.7327	18.8132
9	3	29.7958	29.6725	29.8002
9	6	25.0838	24.9800	25.0874
9	9	17.2297	17.1583	17.2319
10	0	38.3360	38.1774	38.3417
10	3	36.7655	36.6134	36.7709
10	6	32.0539	31.9211	32.0584
10	9	24.2002	24.0999	24.2035
20	0	146.3334	145.7283	146.3548
20	3	144.7645	144.1658	144.7856
20	6	140.0574	139.4781	140.0777
20	9	132.2114	131.6644	132.2304
20	12	121.2253	120.7236	121.2425
20	15	107.0973	106.6538	107.1122
20	18	89.8252	89.4529	89.8372
80	78	1195.6590	1190.7160	1195.8090

has been adopted for the rest of calculations for $^{32}S^{16}O_3$ presented below.

The DMS was calculated using the same level of theory as the PES and on the same grid of 13 000 points. The *ab initio* values were then expressed analytically using the symmetrized molecular bond (SMB) representation described in detail in ref. 32. The resulting dipole moment parameters obtained through a least squares fit reproduce the *ab initio* data with an rms error of 0.00013 D. In these fits the factor defined by eqn (8) was used to weight the geometries according to the corresponding energies. To our knowledge there are no experimental or *ab initio* dipole moment data in the literature that we could use to validate our DMS against. However, our experience of working dipole moments for different systems[33–35] shows that high quality *ab initio* intensities in most cases are competitive with experimental measurements. The quality of the relative intensities calculated using our DMS is discussed below.

The potential energy (both *ab initio* and morphed) and dipole functions used in the present work are given in the ESI.†

III Ro-vibrational calculations

A Basis set convergence and Hamiltonian optimisation

Ro-vibrational calculations for SO_3 were performed using the program TROVE[30] employing the same computational procedures used for the ammonia molecule.[36,37] These molecules share the same molecular symmetry group $D_{3h}(M)$.[38] In order to achieve results of high accuracy as well as to minimise the requirement for computational resources, it is necessary to optimise the size of the Hamiltonian matrix. This involves preliminary truncation of the basis set, as well as limiting the order of both the kinetic and potential components of the Hamiltonian expansion (see ref. 30). Deciding upon these expansion orders involves a trade-off between accuracy and computational expense; it is necessary to initially ensure that the need for computational resource is at a minimum, while maintaining a good degree of accuracy. TROVE employs a polyad number truncation which controls the size of the basis set. For SO_3 the polyad number is given by

$$P = 2(n_1 + n_2 + n_3) + n_4 + n_5 + \frac{n_6}{2}, \qquad (9)$$

where n_i are the quanta associated with 1D basis functions, ϕ_i, whose product gives our vibrational basis set.[30] Each of these basis functions is associated with an internal coordinate ξ_i, and only functions for which $P \leq P_{max}$ are included in the primitive basis set. Initial tests were carried out to measure the degree of convergence using different values for P_{max}, and the orders of the kinetic and potential energy expansions. In this work we use a kinetic energy expansion of order 4, and a potential energy expansion of order 8; using a kinetic energy expansion order of 6 requires a more expensive calculation where convergence is already observed to be within 0.001 cm^{-1} when expanding to fourth order. In the present study, we find that the convergence is more sensitive to P_{max}, and we obtain convergence to within 0.1 cm^{-1} when P_{max} is 12 (see Table 1), we therefore use a basis set based on this value.

As well as using the polyad number to truncate the size of the basis, we employ a further truncation technique by specifying an upper limit for the eigenvalue calculations, *i.e.* the basis set is constructed such that it is approximately associated with energy values up to a limit of E_{max}. This is based on an estimate given by summing eigenvalues of our 1D basis functions before they are considered for matrix element calculations; the active space is constructed using basis functions whose eigenvalues sum together to have $E \leq E_{max}$. For the present study we use E_{max}/hc = 10 000 cm^{-1}.

These precautions are particularly important for the SO_3 molecule, as its larger mass (compared to, for example, XH_3 systems) gives rise to small rotational constants, which in turn requires calculations up to a high J value to ensure adequate coverage of transitions for a given temperature. This means that use of any unnecessary basis functions will prove computationally costly. In addition to this basis set minimisation, we can reduce the size of the Hamiltonian further by making use of the group theory. SO_3 belongs to the $D_{3h}(M)$ molecular group symmetry, which spans six irreducible representations. The nuclear spin-0 Bosons of the constituent atoms allow only the molecular ro-vibrational wavefunctions of the A_1' and A_1'' representations in order to satisfy the Pauli principle. This reduces both the number of Hamiltonian matrices we need to consider and, since E symmetry Hamiltonian matrices are larger, their size.

The two other factors which are important in our spectral calculations are (i) the wavenumber range of the desired synthetic spectrum and (ii) the temperature at which we wish to simulate it. The quality of a computed spectrum will become

sensitive to E_{max} as the temperature increases; we need to ensure that we calculate all energy states that are significantly populated at the given temperature. This can be checked using the temperature-dependent partition function:

$$Q(T) = \sum_i g_i \exp(-E_i/kT), \quad (10)$$

where g_i is the total degeneracy of the ro-vibrational state i with energy E_i, with the sum running over all energies at the absolute temperature T, and k is Boltzmann's constant. The total degeneracy is given by $(2J + 1)$ times the nuclear spin degeneracy, which for the present case of $^{32}S^{16}O_3$ is simply 1 for both the A_1' and A_1'' symmetries, given that the nuclear spin of ^{16}O and ^{32}S is zero. For a given temperature, we can determine the contribution of various states to the value of Q and then check that Q converges to a specific value as E_i tends to infinity; as T increases we require a greater coverage of higher-lying energy states. At T = 298.15 K we find that Q converges to better than 1% at J = 85, with a value of Q = 8089.3. Therefore calculations spanning all J's up to 85 should be sufficient for simulating spectra at this temperature. Fig. 1 shows the value of Q as a function of all energy levels having the J quantum number up to a maximum value, J_{max}, at an absolute temperature of T = 298.15 K. As energies are included in the summation for increasing values of J, we see that the associated energy levels contribute less and less to the value of Q, until it converges to a limit.

An *ab initio* quartic force field was previously published by Martin based on coupled cluster methods.[14] As an initial test of the TROVE procedure we used the force field given by Martin to compute fundamental term values using a well-converged polyad truncation scheme of P_{max} = 16. We found discrepancies between our results and the values published, particularly the value of the ν_2 fundamental term value. We suspected that Marin's F_{22} value has a problem and substituted it with a scaled value from a previously published force-field;[13] this results in a significant improvement. Table 3 illustrates the differences between the values and our final converged result for the fundamental vibrations, and we see that we converge to an improved degree using our morphed PES.

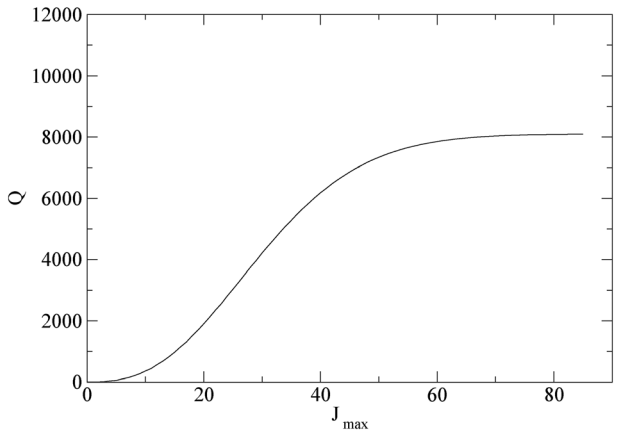

Fig. 1 Convergence of a partition function at 298.15 K for different values of J_{max}.

Table 3 A comparison of the fundamental term values (cm^{-1}) computed with TROVE employing the new morphed PES ('this work'), the original ('Martin') force constants[14] and the F_{22}-corrected[a] ('Martin F_{22}'), see the text

	Obs.[8]	Martin	Martin F_{22}	This work
ν_1	1064.92	1063.36	1064.22	1065.75
ν_2	497.57	428.36	487.10	498.48
ν_3	1391.52	1386.81	1386.85	1387.45
ν_4	530.09	527.35	527.32	528.59

[a] Martin's force constants,[14] with a substituted F_{22} value from ref. 13.

B Intensity simulations

The simulation of absorption spectra can be broken down into two main parts: first, the eigenfunctions and eigenvalues of the numerically constructed Hamiltonian matrix are calculated using a diagonalisation procedure; second, these eigenfunctions are used to compute transition dipoles, line strengths S, Einstein A coefficients and intensities I for allowed transitions. For $^{32}S^{16}O_3$, the rigorous selection rules determining allowed electric dipole transitions are $\Delta J = J' - J'' = 0, \pm 1$ ($J'' + J' \geq 1$), and symmetry selection rules $A_1' \leftrightarrow A_1''$. The intensity of a transition between two states is given by the formula[38]

$$I(\mathrm{f} \leftarrow \mathrm{i}) = \frac{8\pi^3 N_A \nu_{if}}{(4\pi\varepsilon_0)3hc} \frac{e^{-E_i/kT}}{Q(T)} \times \left[1 - \exp\left(\frac{-hc\nu_{if}}{kT}\right)\right] S(\mathrm{f} \leftarrow \mathrm{i}), \quad (11)$$

where I(f ← i) is the transition intensity for a transition from state i with energy E_i to state f with energy E_f, with $hc\nu_{if} = E_f - E_i$. Q is the partition function. S(f ← i) is the line strength, which is defined by the following integration:[38]

$$S(\mathrm{f} \leftarrow \mathrm{i}) = g_{ns} \sum_{m_f, m_i} \sum_{A=X,Y,Z} |\langle \Phi_{rv}^{(f)} | \mu_A | \Phi_{rv}^{(i)} \rangle|^2 \quad (12)$$

for a transition between the initial state i with rovibrational wavefunction $\Phi_{rv}^{(i)}$ and the final state f with wavefunction $\Phi_{rv}^{(f)}$. Here, g_{ns} is the nuclear spin statistical weight factor, and μ_A is the electronically averaged component of the molecular dipole moment along the space-fixed axis $A = X, Y, Z$. The sum also runs over the quantum numbers m_i and m_f which are projections of the total angular momentum J (in units of $\hbar$) on the laboratory fixed Z axis, for the initial and final states, respectively.

Maki *et al.*[5–11] reported extensive high-resolution studies of a number of fundamental, combination and overtone bands of $^{32}S^{16}O_3$. Their principle aim was to obtain accurate wavenumber measurements, but relative intensities were also measured. In the present work we convert these data into absolute intensities by normalizing to the theoretical intensities obtained using TROVE at T = 298.15 K as described below.

The measurements available to us cover three spectral regions: 405–708 cm^{-1} (focusing on the ν_2, ν_4, $2\nu_2 - \nu_2$, $\nu_2 + \nu_4 - \nu_2$, $\nu_2 + \nu_4 - \nu_4$, $\nu_1 - \nu_4$, $2\nu_4^{(l_4=0)} - \nu_4$ and $2\nu_4^{(l_4=2)} - \nu_4$ bands), 1200–1680 cm^{-1} (ν_3), and 2500–3280 cm^{-1} ($2\nu_3^{(l_3=2)}$). These measurements were each made at different values of pressure.

Table 4 Comparison of calculated (TROVE) and experimental[8] band centers and numbers of line transitions

Band	Obs.	Calc.	P_1	P_2	TROVE
$\nu_2 - \nu_0$	497.57	498.48	773	1265	5422
$\nu_4 - \nu_0$	530.09	528.59	996	2052	12 195
$\nu_1 - \nu_4$	534.83	537.16	0	69	15 147
$\nu_2 + \nu_4 - \nu_2$	530.33	528.87	84	571	12 477
$2\nu_2 - \nu_2$	497.45	496.88	112	704	7171
$\nu_2 + \nu_4 - \nu_4$	497.81	498.76	47	602	27 182
$2\nu_4^{(l_4=2)} - \nu_4$	530.36	528.79	116	775	31 096
$2\nu_4^{(l_4=0)} - \nu_4$	529.72	527.91	39	455	13 718
$\nu_3 - \nu_0$	1391.52	1387.45	2014	—	14 441
$2\nu_3^{(l_3=2)} - \nu_0$	2777.87	2770.29	1527	—	18 115
$\nu_0 - \nu_0$	—	—	25	—	3439

[a] For the 405–708 cm^{-1} region, measurements were made at two pressures; P_1 = 0.409 Torr, and P_2 = 2.04 Torr. For the ν_3 and $2\nu_3^{(l_3=2)}$ bands only the lower pressure measurements at 0.16 Torr[8] are used here. Pressure values are not recorded for microwave measurements.[12]

For the 405–708 cm^{-1} window, the measurements were performed at 0.409 and 2.04 Torr. For the ν_3 measurements in the 1200–1680 cm^{-1} window, pressures of 0.16 Torr and 0.7 Torr were used. 560 lines were measured at 0.7 Torr, however 439 of these had relative intensity values which were negative. We therefore do not use this higher pressure measurement at all.

In Table 4 we compare the numbers of lines identified in each measurement to the numbers of lines computed using TROVE. The latter numbers are the subject of the following selection criteria: $J \leq 85$, intensity cut-off, $I(f \leftarrow i) > 10^{-34}$ cm per molecule, and the wavenumber window, 0–4000 cm^{-1}. Experimental lines with negative relative intensities were left out of the analysis.

To normalize the experimental intensities, the experimental relative data obtained from each spectral window and at each different pressure were scaled to match the theoretical values computed at T = 298.15 K. The scaling factors obtained through a minimization procedure using all selected experimental lines with non-zero intensity (see Table 5) are 6.571×10^{-21} cm per molecule (405–708 cm^{-1}, 0.409 Torr), 1.838×10^{-21} cm per molecule (405–708 cm^{-1}, 2.04 Torr), 4.823×10^{-20} cm per molecule (1200–1680 cm^{-1}, 0.16 Torr), and 1.328×10^{-21} cm per molecule (2500–3280 cm^{-1}, 4.99 Torr). With these factors the 'experimental' intensities match the theoretical values reasonably well, for example for 405–708 cm^{-1} the agreement is within about 7.02×10^{-22} cm per molecule and 5.05×10^{-22} cm per molecule, at 0.409 and 2.04 Torr, respectively.

Having the absolute intensities derived, band intensities were estimated for each experimental band as the sum of individual line intensities. In Table 5 these 'experimental' band intensities S^{exp} (cm per molecule) are compared to the theoretical values obtained by summing intensities (a) from all TROVE lines from a given window and (b) only from lines with experimental counterparts present. This was done separately for each spectral range, and each measurement pressure therein. In Table 5 these quantities are referenced to as S_{tot}^{calc} and S_{red}^{calc} for the 'total' and 'reduced' band intensities, respectively, and compared to S^{exp}. The ratio S_{red}^{calc} to S^{exp} also shown in Table 5 demonstrates the good quality of the scaling procedure employed as well as that of our dipole moment. For example at 0.409 Torr, the differences between 'experimental' and theoretical band intensities are within about 20% for all bands from the 405–708 cm^{-1} region with the exception of $2\nu_4^{(l_4=0)} - \nu_4$ (see also discussion below). It should be stressed here that only one scaling factor for all eight bands from this window was applied at a given pressure. The difference between the two theoretical band intensities S_{tot}^{calc} and S_{red}^{calc} gives a measure of the missing experimental transition data. According to Table 5 the measurements for even stronger bands are missing more than 50% of the total intensity.

Table 5 also shows theoretical values of vibrational transition moments defined as

$$\bar{\mu} = \sqrt{\bar{\mu}_x^2 + \bar{\mu}_y^2 + \bar{\mu}_z^2}, \quad (13)$$

where

$$\bar{\mu}_\alpha = \langle \Psi_{vib}^{(i)} | \mu_\alpha | \Psi_{vib}^{(f)} \rangle, \quad (14)$$

and $\Psi_{vib}^{(i)}$ and $\Psi_{vib}^{(f)}$ are the vibrational eigenfunctions of the 'initial' and 'final' states, respectively, variationally computed

Table 5 Vibrational band intensities S^{exp}, S_{tot}^{calc}, S_{red}^{calc} in cm per molecule $\times 10^{-18}$, and calculated transition moments $\bar{\mu}_{if}$ in Debye. P_1 and P_2 refer to the different pressure measurements within the same wavenumber region (see Table 4). S_{red}^{calc}/S^{exp} is the ratio of the theoretical reduced and total band intensities (see the text). S_{tot}^{calc} is the theoretical band intensity computed by summing all TROVE lines. S^{exp} is the experimental band intensity obtained from a summation over all experimental values after scaling factors are applied (see the text). S_{red}^{calc} is the theoretical band intensity computed using only lines for which experimental counterparts exist. N_{red} is the number of matched lines

	S^{exp}			S_{red}^{calc}		S_{red}^{calc}/S^{exp}		N_{red}		
Band	P_1	P_2	S_{tot}^{calc}	P_1	P_2	P_1	P_2	P_1	P_2	$\bar{\mu}_{if}$/D
ν_2	2.987	1.537	3.705	2.915	1.559	0.98	1.01	773	1265	0.158
ν_4	4.258	3.112	5.949	4.310	3.149	1.01	1.01	995	2052	0.200
$2\nu_2 - \nu_2$	0.116	0.470	0.661	0.101	0.411	0.88	0.88	112	704	0.221
$\nu_2 + \nu_4 - \nu_2$	0.062	0.322	0.528	0.052	0.251	0.84	0.78	84	571	0.199
$\nu_2 + \nu_4 - \nu_4$	0.026	0.260	0.581	0.022	0.215	0.84	0.83	47	602	0.223
$2\nu_4(l_4 = 2) - \nu_4$	0.112	0.589	0.873	0.102	0.485	0.91	0.82	116	769	0.283
$2\nu_4(l_4 = 0) - \nu_4$	0.026	0.222	0.405	0.015	0.179	0.57	0.81	38	454	0.196
$\nu_1 - \nu_4$	—	0.009	0.101	—	0.003	—	0.29	—	69	0.039
ν_3	39.490	—	44.440	39.490	—	—	—	2014	—	0.321
$2\nu_3$	0.093	—	0.119	0.093	—	—	—	1527	—	0.012

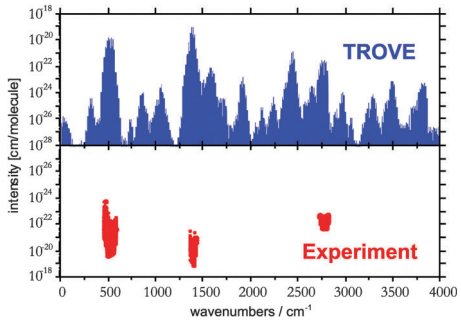

Fig. 2 Overview of the simulated absorption (T = 298.15 K) spectrum (TROVE) of SO_3 compared to experiment scaled to the theoretical intensities (see the text).

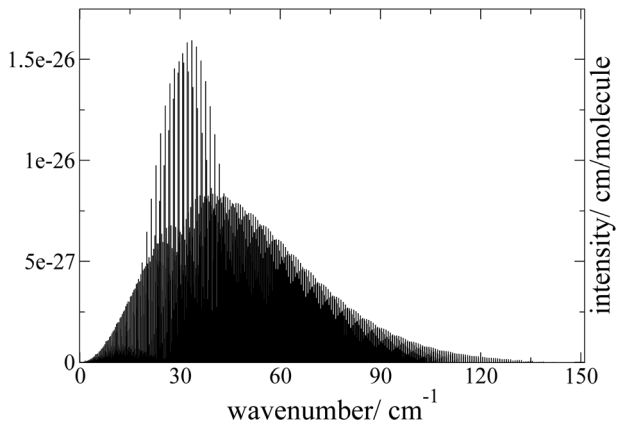

Fig. 3 Rotational absorption band computed for T = 298.15 K, complete up to J = 85.

using TROVE and μ_α is the component of the molecular dipole moment along the molecular-fixed axis $\alpha = x, y, z$.

Fig. 2 presents an overview of the simulated spectrum (T = 298.15 K) using TROVE and experimental absorption spectra of $^{32}S^{16}O_3$ for the whole simulation range up to 4000 cm^{-1}. It reveals the gaps and limitations of the available experimental data. Fig. 3 shows the 'forbidden' rotational band as a stick spectrum. It should be noted that the microwave measurements of ref. 12 do not report any intensities. In Fig. 4 all eight bands from the 405–708 cm^{-1} region are combined into one graph for each pressure to illustrate the quality of the corresponding experimental data. This figure suggests that the 0.409 Torr data are generally more reliable. This is also reflected by the ratio values $S_{\mathrm{red}}^{\mathrm{calc}}/S^{\mathrm{exp}}$ from Table 5, which are significantly closer to 1 at the lower pressure. For data obtained at two pressures we therefore consider scaled intensity values obtained at the lower pressure to be more reliable. Finally, Fig. 5 presents a detailed comparison for all the bands from the three spectral regions studied in this work in the form of stick diagrams. Our intensities based on the *ab initio* DMS are in very good qualitative agreement with the experiment.

IV Conclusions and discussions

The shifted theoretical bands in Fig. 4 and 5 indicate that our morphed PES of SO_3 requires further improvement (see also band

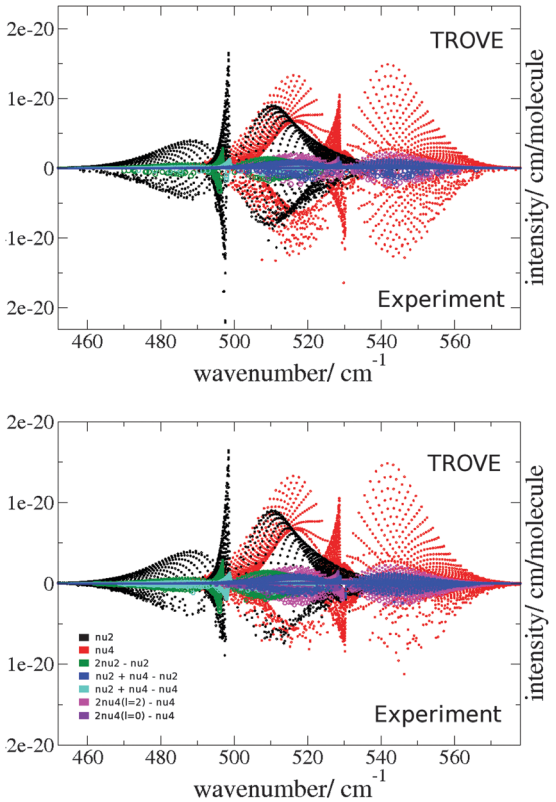

Fig. 4 Comparison plot of TROVE results and the bands of interest measured between 405–708 cm^{-1} by Maki *et al.*, at 0.409 Torr (above) and 2.04 Torr (below). Points are enlarged in some cases for clarity.

centers in Table 4). The theoretical ν_2 frequencies have an rms deviation of 0.91 cm^{-1} when compared with the experimental data, which is relatively small compared to the deviation for ν_3 of 4.07 cm^{-1}. This is to be expected since the underlying *ab initio* PES was computed at a modest level of theory. We are planning to refine this surface by fitting to all experimental data available.

Table 5 outlines the quality of the intensity scaling procedure, in which the relative values of the experimental intensities were converted to absolute values (cm per molecule). For the 0.409 Torr and 2.04 Torr measurements our comparisons mostly agree to within 20%, with the exception of the $2\nu_4^{(l_4=0)} - \nu_4$ band measured at 0.409 Torr which shows nearly a 50% difference, and the $\nu_1 - \nu_4$ band measured at 2.04 Torr with 80% uncertainty. The latter can probably be attributed to both the small number of lines in each case, and residual errors in the transition dipole. In the case of the $2\nu_4^{(l_4=0)} - \nu_4$ band the comparison with the 2.04 Torr experiment yields a better value for $S_{\mathrm{red}}^{\mathrm{calc}}/S^{\mathrm{exp}}$ than for the 0.409 Torr measurement, which suggests that the number of lines available at 0.409 Torr is too low (see also Fig. 4). The significance of the results presented in Table 5 and illustrated in Fig. 4 is that these give an estimation on the quality of the *ab initio* dipole moment surface as well as of the experimental data. Based on these numbers we can place a lower estimate on the quality uncertainty for our intensities for each band, for example the experiment and theory for the ν_2 and ν_4 bands agree at least to within 3%

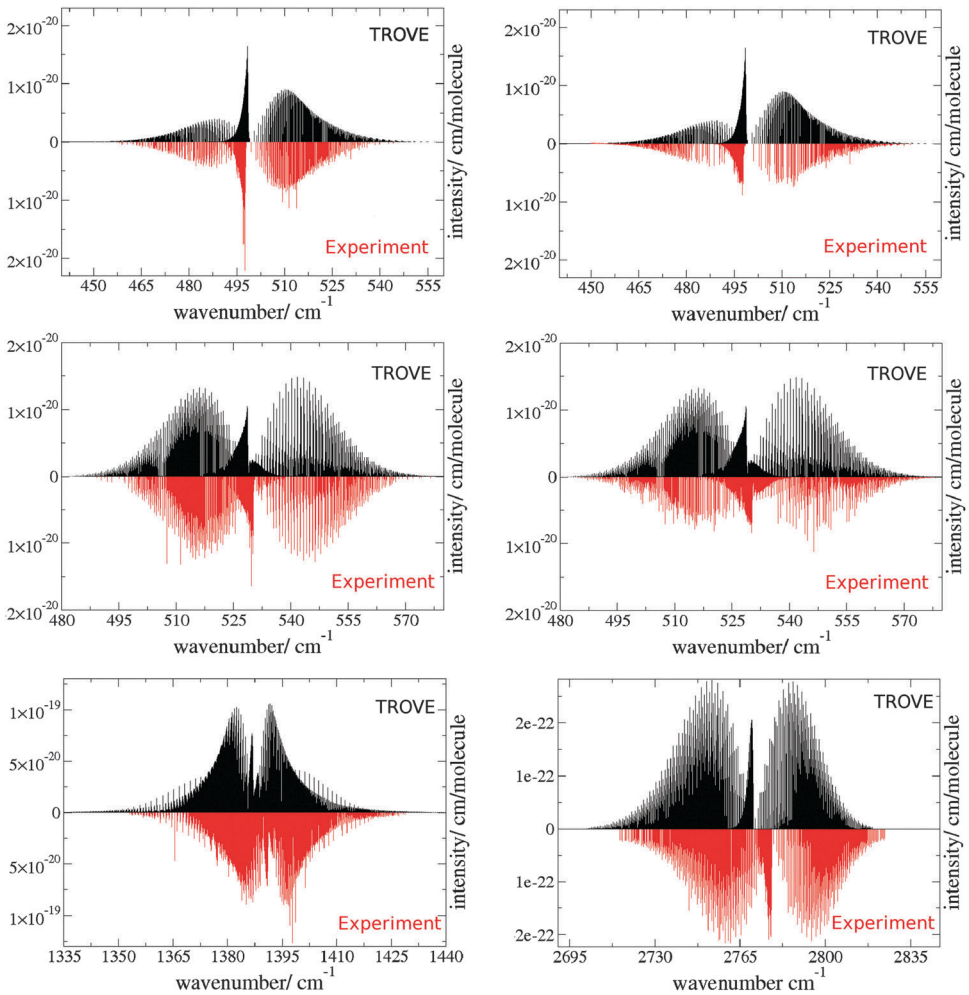

Fig. 5 Fundamental band comparisons between this work (T = 298.15 K, complete up to J = 85) and Maki *et al.*[8] The top and middle panels show comparisons for the ν_2 and ν_4 bands, respectively, at 0.409 Torr (left) and 2.04 Torr (right). The bottom panel shows a comparison for the ν_3 band at 0.16 Torr (left) and the $2\nu_3$ band at 4.99 Torr (right).

for both pressure measurements, while it is only 13% for $2\nu_2 - \nu_2$, and about 18% for the remaining bands.

Our complete room-temperature line list for SO_3 containing 174 674 257 transitions can be accessed online at www.exomol.com in the ExoMol format described in ref. 39. It includes the transition energies, Einstein coefficients A(f ← i), and absorption intensities estimated for T = 298.15 K. Additionally, a list of 10 878 experimental transitions with absolute intensities obtained for T = 296 K is included in the ESI† part of this paper in a form suitable for standard atmospheric and planetary spectroscopic databases.

Our future work will be focused on the development of a hot line list for $^{32}S^{16}O_3$ for high temperature industrial applications as well as for modelling molecular opacity in atmospheres of (exo-)planets and cool stars as part of the ExoMol project[40] (see www.exomol.com).

Acknowledgements

We thank Alexander Fateev for stimulating our interest in this molecule and for many helpful discussions, and Jeff Barber for supplying his experimental result. This work was supported by grant 10442 from energinet.dk under a subcontract from the Danish Technical University and the ERC under Advanced Investigator Project 267219.

References

1 W. T. Rawlins, J. M. Hensley, D. M. Sonnenfroh, D. B. Oakes and M. G. Allen, *Appl. Opt.*, 2005, **44**, 6635–6643.
2 D. Fleig, E. Vainio, K. Andersson, A. Brink, F. Johnsson and M. Hupa, *Energy Fuels*, 2012, **26**, 5537–5549.
3 J. P. Michaud, D. Krupitsky, J. S. Grove and B. S. Anderson, *NeuroToxicology*, 2005, **26**, 555–563.
4 X. Zhang, M.-C. Liang, F. Montmessin, J.-L. Bertaux, C. Parkinson and Y. L. Yung, *Nat. Geosci.*, 2010, **3**, 834–837.
5 A. Kaldor, A. G. Maki, A. J. Dorney and I. M. Mills, *J. Mol. Spectrosc.*, 1973, **45**, 247–252.
6 J. Ortigoso, R. Escribano and A. G. Maki, *J. Mol. Spectrosc.*, 1989, **138**, 602–613.
7 E. T. H. Chrysostom, N. Vulpanovici, T. Masiello, J. Barber, J. W. Nibler, A. Weber, A. Maki and T. A. Blake, *J. Mol. Spectrosc*, 2001, **210**, 233–239.

8 A. Maki, T. A. Blake, L. S. Sams, N. Vulpanovici, J. Barber, E. T. H. Chrysostom, T. Masiello, J. W. Nibler and A. Weber, *J. Mol. Spectrosc.*, 2001, **210**, 240–249.
9 J. Barber, E. T. H. Chrysostom, T. Masiello, J. W. Nibler, A. Maki, A. Weber, T. A. Blake and R. L. Sams, *J. Mol. Spectrosc.*, 2002, **216**, 105–112.
10 S. W. Sharpe, T. A. Blake, R. L. Sams, A. Maki, T. Masiello, J. Barber, N. Vulpanovici, J. W. Nibler and A. Weber, *J. Mol. Spectrosc.*, 2003, **222**, 142–152.
11 A. Maki, T. A. Blake, R. L. Sams, J. Frieh, J. Barber, T. Masiello, E. T. H. Chrysostom, J. W. Nibler and A. Weber, *J. Mol. Spectrosc.*, 2004, **225**, 109–122.
12 V. Meyer, D. H. Sutter and H. Dreizler, *Z. Naturforsch., A: Phys. Sci.*, 1991, **46**, 710–714.
13 A. J. Dorney, A. R. Hoy and I. M. Mills, *J. Mol. Spectrosc.*, 1973, **45**, 253–260.
14 J. M. L. Martin, *Spectrochim. Acta, Part A*, 1999, **55**, 709–718.
15 L. S. Rothman, I. E. Gordon, A. Barbe, D. C. Benner, P. F. Bernath, M. Birk, V. Boudon, L. R. Brown, A. Campargue, J. P. Champion, K. Chance, L. H. Coudert, V. Dana, V. M. Devi, S. Fally, J. M. Flaud, R. R. Gamache, A. Goldman, D. Jacquemart, I. Kleiner, N. Lacome, W. J. Lafferty, J. Y. Mandin, S. T. Massie, S. N. Mikhailenko, C. E. Miller, N. Moazzen-Ahmadi, O. V. Naumenko, A. V. Nikitin, J. Orphal, V. I. Perevalov, A. Perrin, A. Predoi-Cross, C. P. Rinsland, M. Rotger, M. Simeckova, M. A. H. Smith, K. Sung, S. A. Tashkun, J. Tennyson, R. A. Toth, A. C. Vandaele and J. V. Auwera, *J. Quant. Spectrosc. Radiat. Transfer*, 2009, **110**, 533–572.
16 N. Jacquinet-Husson, L. Crepeau, R. Armante, C. Boutammine, A. Chdin, N. A. Scott, C. Crevoisier, V. Capelle, C. Boone, N. Poulet-Crovisier, A. Barbe, A. Campargue, D. C. Benner, Y. Benilan, B. Bzard, V. Boudon, L. R. Brown, L. H. Coudert, A. Coustenis, V. Dana, V. M. Devi, S. Fally, A. Fayt, J.-M. Flaud, A. Goldman, M. Herman, G. J. Harris, D. Jacquemart, A. Jolly, I. Kleiner, A. Kleinbhl, F. Kwabia-Tchana, N. Lavrentieva, N. Lacome, L.-H. Xu, O. M. Lyulin, J.-Y. Mandin, A. Maki, S. Mikhailenko, C. E. Miller, T. Mishina, N. Moazzen-Ahmadi, H. S. P. Mller, A. Nikitin, J. Orphal, V. Perevalov, A. Perrin, D. T. Petkie, A. Predoi-Cross, C. P. Rinsland, J. J. Remedios, M. Rotger, M. A. H. Smith, K. Sung, S. Tashkun, J. Tennyson, R. A. Toth, A.-C. Vandaele and J. V. Auwera, *J. Quant. Spectrosc. Radiat. Transfer*, 2011, **112**, 2395–2445.
17 T. Adler, G. Knizia and H.-J. Werner, *J. Chem. Phys.*, 2007, **127**, 221106.
18 K. Yousaf and K. Peterson, *Chem. Phys. Lett.*, 2009, **476**, 303.
19 K. Yousaf and K. Peterson, *J. Chem. Phys.*, 2008, **129**, 184108(7 pp.).
20 F. Weigend, *Phys. Chem. Chem. Phys.*, 2002, **4**, 4285–4291.
21 C. Hättig, *Phys. Chem. Chem. Phys.*, 2005, **7**, 59–66.
22 H. J. Werner, P. J. Knowles, R. Lindh, F. R. Manby and M. Schütz, *et al.*, *MOLPRO, a package of ab initio* programs, 2010, see http://www.molpro.net/.
23 T. J. Lee and P. R. Taylor, *Int. J. Quantum Chem.*, 1989, 199–207.
24 S. N. Yurchenko, M. Carvajalz, P. Jensen, H. Lin, J. J. Zheng and W. Thiel, *Mol. Phys.*, 2005, **103**, 359–378.
25 H. Lin, W. Thiel, S. N. Yurchenko, M. Carvajal and P. Jensen, *J. Chem. Phys.*, 2002, **117**, 11265–11276.
26 S. N. Yurchenko, W. Thiel and P. Jensen, *J. Mol. Spectrosc.*, 2006, **240**, 174–187.
27 R. I. Ovsyannikov, W. Thiel, S. N. Yurchenko, M. Carvajal and P. Jensen, *J. Mol. Spectrosc.*, 2008, **252**, 121–128.
28 S. N. Yurchenko, W. Thiel, M. Carvajal and P. Jensen, *Chem. Phys.*, 2008, **346**, 146–159.
29 H. Partridge and D. W. Schwenke, *J. Chem. Phys.*, 1997, **106**, 4618–4639.
30 S. N. Yurchenko, W. Thiel and P. Jensen, *J. Mol. Spectrosc.*, 2007, **245**, 126–140.
31 S. Skokov, K. A. Peterson and J. M. Bowman, *Chem. Phys. Lett.*, 1999, **312**, 494–502.
32 S. N. Yurchenko, R. J. Barber and J. Tennyson, *Mon. Not. R. Astron. Soc.*, 2011, **413**, 1828–1834.
33 A. E. Lynas-Gray, S. Miller and J. Tennyson, *J. Mol. Spectrosc.*, 1995, **169**, 458–467.
34 L. Lodi, J. Tennyson and O. L. Polyansky, *J. Chem. Phys.*, 2011, **135**, 034113.
35 S. N. Yurchenko, J. Tennyson, R. J. Barber and W. Thiel, *J. Mol. Spectrosc.*, 2013, submitted.
36 S. N. Yurchenko, R. J. Barber, A. Yachmenev, W. Thiel, P. Jensen and J. Tennyson, *J. Phys. Chem. A*, 2009, **113**, 11845–11855.
37 S. N. Yurchenko, R. J. Barber and J. Tennyson, *Mon. Not. R. Astron. Soc.*, 2011, **413**, 1828–1834.
38 P. Jensen and P. R. Bunker, *Molecular Symmetry and Spectroscopy*, NRC, Canada, 1998.
39 M. line lists for the opacity of exoplanets and other atmospheres, Eighth International Conference on Atomic and Molecular Data and Their Applications: ICAMDATA-8, 2012.
40 J. Tennyson and S. N. Yurchenko, *Mon. Not. R. Astron. Soc.*, 2012, **425**, 21–33.